Hydrodynamics and Free-Flow Characteristics of Piano Key Weirs with Different Plan Shapes

Yousef Sangsefidi [1], Hassan Tavakol-Davani [1], Masoud Ghodsian [2,*], Mojtaba Mehraein [3] and Reza Zarei [4]

1 Urban Water Group, San Diego State University, San Diego, CA 92182, USA; ysangsefidi@ucsd.edu (Y.S.);
   htavakol@sdsu.edu (H.T.-D.)
2 Water Engineering Research Institute, Faculty of Civil and Environmental Engineering,
   Tarbiat Modares University, Tehran P.O. Box 14115-114, Iran
3 Faculty of Engineering, Kharazmi University, Tehran 15719-14911, Iran; mehraein@khu.ac.ir
4 Water Engineering and Hydraulic Structures, Faculty of Civil and Environmental Engineering,
   Tarbiat Modares University, Tehran P.O. Box 14115-114, Iran; z.reza@modares.ac.ir
* Correspondence: ghods@modares.ac.ir

Abstract: This paper focuses on Piano Key Weirs (PKWs) as an effective solution for improving the discharge capacity of spillway systems. The flow behavior in inlet and outlet keys is experimentally studied to analyze the discharge capacity of PKWs with different plan shapes (i.e., rectangular, trapezoidal, and triangular). The results show that in outlet keys, the flow aeration regimes extend to higher values of headwater ratios (H_o/P) by increasing the length magnification ratio (B/w) and apex width ratio (A/w). In addition, the local submergence length is a decreasing function of A/w, especially in high flow heads. While the total interference length enlarges by reducing A/w in lower H_o/P values ($H_o/P < 0.5$), a reverse trend is observed in higher headwater ratios. PKW performance may also be impacted by the flow contraction and recirculation zone in inlet keys, which intensify in higher values of H_o/P, B/w, and A/w. According to the obtained results, while the discharge coefficient is a decreasing function of A/w in $H_o/P > 0.4$, it may have a reverse trend in lower head conditions. In addition, a trapezoidal PKW has the highest discharge efficiency in a wide range of the studied domain ($H_o/P > 0.25$ and $B/w \geq 2$). It can improve the discharge efficiency by around 5%, while its body volume is almost 7% smaller than the traditional rectangular PKW. However, for low-length and high-head conditions ($B/w = 1$ and $H_o/P > 0.5$), the efficiency a rectangular PKW exceeds that of the other shapes.

Keywords: piano key weir; flow behavior; discharge capacity; plan shape; weir length
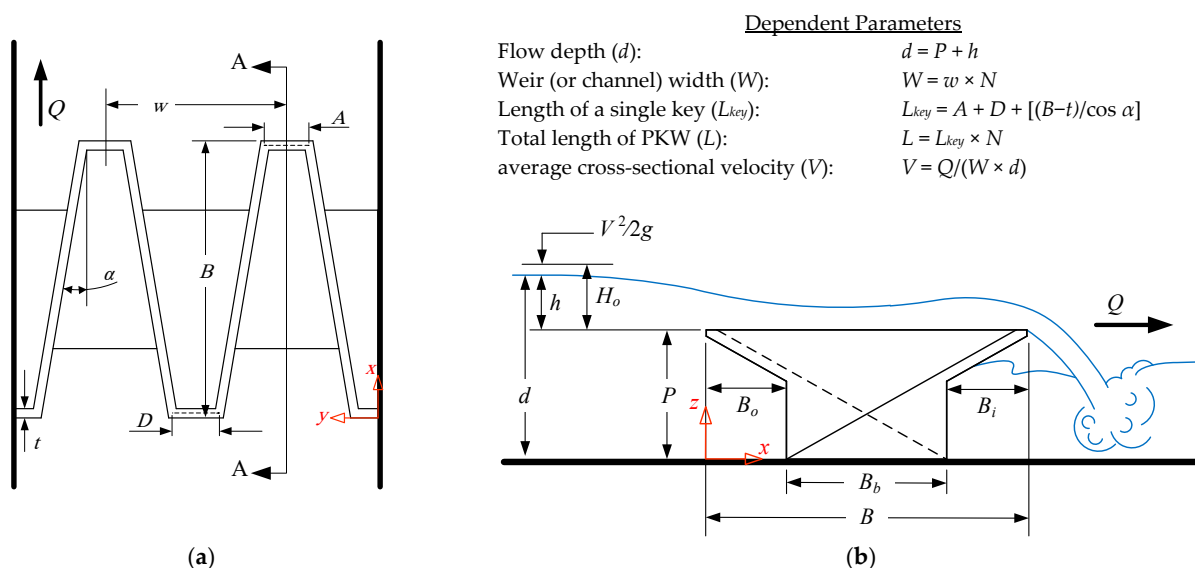
1. Introduction

Spillways play an essential role in the safety and service of water reservoirs; they are designed to safely pass floods, especially after considering the growing climate change effects leading to more extreme flood events [1]. A survey of US Army Corps of Engineers indicates that ~30% of existing dams are currently unsafe due to having inadequate spillway capacity [2]. This shortcoming has been the cause of one-third of dam failures that has resulted in huge life and financial losses [3]. As a recent example, in May 2020, the collapse of Edenville Dam in Michigan, USA forced thousands of people to evacuate [4].

In response to the required rehabilitation of dam reservoirs and their aged and inefficient structures, innovative solutions have been developed by researchers to allow the structures to meet the safe passage of floods and increased water demands. A nonlinear weir with a folded crest in plan view improves the discharge capacity of spillway systems by extending the crest length for a given channel width. It can be an economical and effective solution for those sites where the structure width is limited while a large discharge capacity is required [5]. In addition, a nonlinear weir can reduce the upstream water head and land submergence compared to conventional water storage diversion systems [6].

Moreover, as low-head control structures, they can also be used in river restoration projects to provide low-velocity regions that are potentially conducive to fish passage [7].

Labyrinth weirs are a classic type of nonlinear weir with vertical walls with different plan shapes such as rectangular [8], trapezoidal [9], triangular [10], semicircular [11], duckbill [12], or arced [13]. Labyrinth weirs have been extensively used in water engineering projects (around 100 constructed prototypes across the globe) [14]. At the beginning of the current century, an innovative and efficient modification, known as Piano Key Weir (PKW), was proposed and included sloped floors and cantilevered apexes into a rectangular labyrinth weir [15].

By comparing a rectangular labyrinth and piano key weirs with the same length, Anderson and Tullis (2012) showed that the PKW discharge coefficient was ~8% larger, which is associated with an increased wetted perimeter, causing a reduction in head loss and making room for the passing flow in the inlet and outlet keys, respectively [16]. More importantly, compared to a traditional labyrinth weir, a PKW accommodates a smaller footprint length (B_b in Figure 1). Thus, it allows a significant increase in the crest length (and discharge capacity) for a given spillway footprint base [16–18]. These features may overcome both restrictions in the length and width of a spillway footprint and may even allow for the implementation of PKWs in challenging situations such as the top of concrete dams or steep, narrow streams. The mentioned advantages have made PKWs an efficient alternative for reservoir management projects (construction of ~30 PKWs during the last decade) [14].

Dependent Parameters

Flow depth (d):	$d = P + h$
Weir (or channel) width (W):	$W = w \times N$
Length of a single key (L_{key}):	$L_{key} = A + D + [(B-t)/\cos \alpha]$
Total length of PKW (L):	$L = L_{key} \times N$
average cross-sectional velocity (V):	$V = Q/(W \times d)$

(**a**) (**b**)

Figure 1. PKW schematic: (**a**) plan view; (**b**) section view A-A.

Regarding the rapid development of PKWs, there has been an apparent link between research and industry projects. In addition to several publications in scientific journals, three international conferences (i.e., PKW2011 (Liège, Belgium), PKW2013 (Paris, France), and PKW2017 (Qui Nhơn, Vietnam)) were held in the last decade, specifically focusing on advancements in PKWs [19–21]. From a selection of the prominent research studies, Lempérière (2013), Laugier et al. (2011), Leite Ribeiro et al. (2012), Kabiri-Samani and Javaheri (2012), Anderson and Tullis (2013), Cicero and Delisle (2013), and Machiels et al. (2014) conducted parametric studies on rectangular PKWs (including but not limited to headwater ratio (H_o/P), weir length magnification ratio (L/W or B/w), wall thickness ratio (t/P), inlet-to-outlet width ratio (A/D), inlet-to-outlet overhang ratio (B_i/B_o), crest shape, and cycle width ratio (w/P)) and provided some recommendations for the selection of their involved parameters [17,22–27]. While the majority of constructed prototypes and conducted research models (including the above-mentioned) have featured a rectangular

shape, the PKW literature shows that the plan shape significantly affects its performance. By comparing a trapezoidal PKW to a traditional rectangular one, Safarzadeh and Noroozi (2017) indicated that a trapezoidal PKW can be approximately 20% more efficient than an ordinary rectangular one with an identical magnification ratio ($L/W \approx 5$) [28]. This point has been proven by the experimental studies of Mehboudi et al. (2016) [29]. Cicero et al. (2013) showed that the gain in discharge may be limited to 5% in high head conditions ($H_o/P > 0.8$) [30].

The literature review also indicates that previous studies have mostly focused on the determination of the head–discharge relationship of PKWs, with relatively few studies examining the effects of flow physics and hydrodynamics on a PKW. The experiments by Machiels et al. (2011) on a large-scale rectangular PKW (P = 52.5 cm) revealed that due to the sharp-corner entrance, a recirculation zone may form in the inlet key of a rectangular PKW [31]. The simulations of Li et al. (2020) and Safarzadeh and Noroozi (2017) confirmed the recirculation zone formation in a rectangular PKW, which enlarges and results in higher heads, leading to a reduction in the inlet key effective area [28,32]. Denys et al. (2017) and Denys (2019) investigated the specifications of the recirculation zone in more detail [33,34]. The three-dimensional numerical simulations showed that a PKW creates two different recirculation zones near its base and crest with the nearly vertical and horizontal rotation axes, respectively. It is worth noting that the 5–15% efficiency gains of the inclusion of an upstream nose [35,36] may be due to limiting the recirculation zone development caused by a more gradual transition at the entrance to the inlet keys. Denys and Basson (2020) showed that due to the formation of the recirculation zone, the upstream face of the rectangular PKW sidewall experiences significant pressure fluctuations (with an average amplitude of ~10% of the total hydrostatic pressure) [37]. According to Kumar et al. (2021), a sediment particle accelerates along the inlet key due to the flow contraction and an increase in shear stress [38]. Regardless of the limited ranges of the above-mentioned studies, they imply that the understanding of the complex flow structure (fundamental research) and the analysis of its possible relation to the discharge capacity (applied research) may clarify PKW benefits and limitations.

Since much of the passing flow over a PKW discharges into outlet keys [39], nappe behavior in this area should be also taken into account when analyzing their performance. Although there is significant information regarding nappe behavior in labyrinth weirs (i.e., aeration conditions, nappe interference and instability, and nappe breaker effects), less data have been provided for PKWs. Through his studies of ~40 rectangular PKW models, Machiels (2012) showed that as the nappe interference zone rises above the crest elevation, the local submergence reduces the inlet key discharge and velocity [40]. By increasing H_o/P, the control section in the outlet keys moves in the downstream direction (also occurs by increasing A/D). Crookston and Tullis (2012) and Crookston and Tullis (2013) studied aeration, instability, and nappe interference in trapezoidal labyrinth weirs [41,42]. Defining different nappe aeration conditions, they stated that when the nappe clings to the downstream surface of the weir, some undesirable conditions such as vibrations, noise, and pressure fluctuations may occur due to subatmospheric pressures under the nappe. Focusing on the flow characteristics over a semicircular labyrinth weir, Bilhan et al. (2018) showed that the subatmospheric pressures can be significantly diminished due to the use of nappe breakers [11]. Bilhan et al. (2018) then estimated the discharge coefficient of trapezoidal labyrinth weirs with/without nappe breakers [43]. The experimental studies of Mehboudi et al. (2017) indicated that trapezoidal PKWs experience aerated and drowned flow regimes when $H_o/P < 0.18$ and $H_o/P > 0.35$, respectively [44]. The corresponding values for rectangular PKWs were reported as $H_o/P < 0.15$ and $H_o/P > 0.2$ by Kabiri-Samani and Javaheri (2012) [25]. According to Vermeulen et al. (2017), although air pockets can exist on the downstream normal walls and sidewalls of a PKW, they is less prone to the resonance phenomenon (due to having folded and sloped walls) compared to a flap gate [45]. Besides the use of nappe breakers and crest roughness, Lombaard (2020) recommended artificial aeration to reduce the intensity of the fluctuations if nappe oscillations are expected for

low head conditions ($H_o/P \leq 0.1$) [46]. In high head conditions, the pressure fluctuations in outlet keys diminish due to the momentum of the accelerated flow.

Due to the multiplicity of effective parameters and the complexity of flow patterns, the performance of PKWs merits more investigation. The literature review has shown that there is still a strong necessity for fundamental and applied research on PKWs, which can improve the comprehension of flow structure around these weirs, and subsequently, set up efficient rules for their design. In the broad ranges of the two main effective parameters (i.e., headwater ratio and weir length magnification ratio), this research evaluates the flow behavior around PKWs for different plan shapes (i.e., rectangular, trapezoidal, and triangular). Its principal objectives are:

- to gain new insights into PKW flow physics through studying water surface profiles and velocity fields in inlet keys and nappe aeration and interference in outlet keys;
- to estimate the discharge capacity of PKWs with different plan shapes and analyze their performance based on the findings and observations of the complex flow structure.

2. Effective Parameters

The PKW discharge can be determined using the following equation [16]:

$$Q = \frac{2}{3} C_d L \sqrt{2g} H_o^{1.5} \tag{1}$$

where Q = weir discharge, C_d = discharge coefficient, L = total length of PKW, g = acceleration due to gravity, and H_o = total upstream head = $h + V^2/2g$ (h is the approach flow depth over the weir, and V is the average cross-sectional velocity of approaching flow). The independent parameters affecting the PKW discharge can be presented as:

$$Q = f(H_o, P, B, w, B_i, B_o, A, D, N, t, g, \rho, \mu, \sigma, S_o, S_e) \tag{2}$$

where f is a functional symbol, P = weir height, B = weir length in streamwise direction, w = cycle width, B_i = inlet key (or downstream) overhang length, B_o = outlet key (or upstream) overhang length, A = inlet key (or downstream) apex width, D = outlet key (or upstream) apex width, N = number of keys, t = weir wall thickness, ρ = fluid density, μ = dynamic viscosity, σ = surface tension, S_o = longitudinal bed slope, and S_e represents the crest shape. Besides These parameters, their dependent parameters are shown in Figure 1.

Using the dimensional analysis, one can derive:

$$C_d = \varphi\left(R, W, \frac{H_o}{P}, \frac{B}{w}, \frac{w}{P}, \frac{B_i}{B}, \frac{B_o}{B}, \frac{A}{w}, \frac{A}{D}, \frac{t}{P}, N, S_o, S_e \right) \tag{3}$$

where φ is another functional symbol, and R = $\rho V d/\mu$ and W = $V(\rho d/\sigma)^{0.5}$ are the Reynolds and Weber numbers of the approach flow, respectively (Figure 1 presents V and d as dependent parameters). Since the viscosity effects are insignificant (turbulent flow with R > 25000), R is eliminated from Equation (3) [47,48]. In lower values of the flow depth, surface tension may affect Froude-scaled models [49]. Pfister et al. (2013) and Erpicum et al. (2016) specifically recommended $h \geq 0.03$ m to avoid these effects on the head–discharge relationship of PKWs [50,51]. The above recommendations have been satisfied in the collection of data; therefore, W (in the range of $7-50$) was also removed from Equation (3). In addition, the geometric parameters of w/P, B_i/B, B_o/B, A/D, t/P, N, S_o, and S_e were constant in this study (note that the values of w/P, A/D, t/P, N, and S_e are different between the base and other models (mentioned in the next section)). Thus, removing these parameters from Equation (3) gives:

$$C_d = \varphi\left(\frac{H_o}{P}, \frac{B}{w}, \frac{A}{w} \right) \tag{4}$$

The present study analyzes the effects of these parameters on the performance of PKWs.

3. Experimental Method

To conduct the experiments, a recirculating flume (10 m long, 2 m wide, and 0.9 m deep) was implemented at the Hydraulic Laboratory of Tarbiat Modares University, Tehran, Iran. As shown in Figure 2, the channel was contracted to a width of 0.75 m using a converging transition. The tested weirs were located within a 1-meter distance from the contracted channel downstream end, where inflow disturbances were effectively damped, and flow under riverine approach conditions were achieved [52]. The discharges (in the range of 0.020−0.185 m³/sec) were determined using two calibrated portable ultrasonic flow meters (TFM3100-F1) with an accuracy of ±1% attached to the inflow pipes. They were recorded during 5–7 min time steps, and the mean values were used for further analyses [53]. Water surface elevations were measured using a Mitutoyo digital point gauge (±0.1 mm accuracy). To calculate the total hydraulic heads, water surface elevations were measured at a minimum of $3h$ upstream from the weir, where the upstream water surface curvature (due to the drawdown effect) is negligible [54]. Flow velocities were measured using Nortek−Vectrino Acoustic Doppler Velocimetry (ADV) with ±0.5% accuracy, in which the sampling duration was 2 minutes at a frequency of 200 Hz. Using WinADV software [55], phase space threshold despiking along with the SNR > 15 and CC > 0.7 was used to filter the contaminated time series (SNR is the signal-to-noise ratio, and CC is the correlation coefficient). Side-looking and down-looking probes were used to measure the flow velocities in different regions around PKW, especially near the vertical walls and the sloped floors (Figure 3). The flow visualizations were recorded using dye injection and a camera with a 14.1 Mega Pixel resolution.
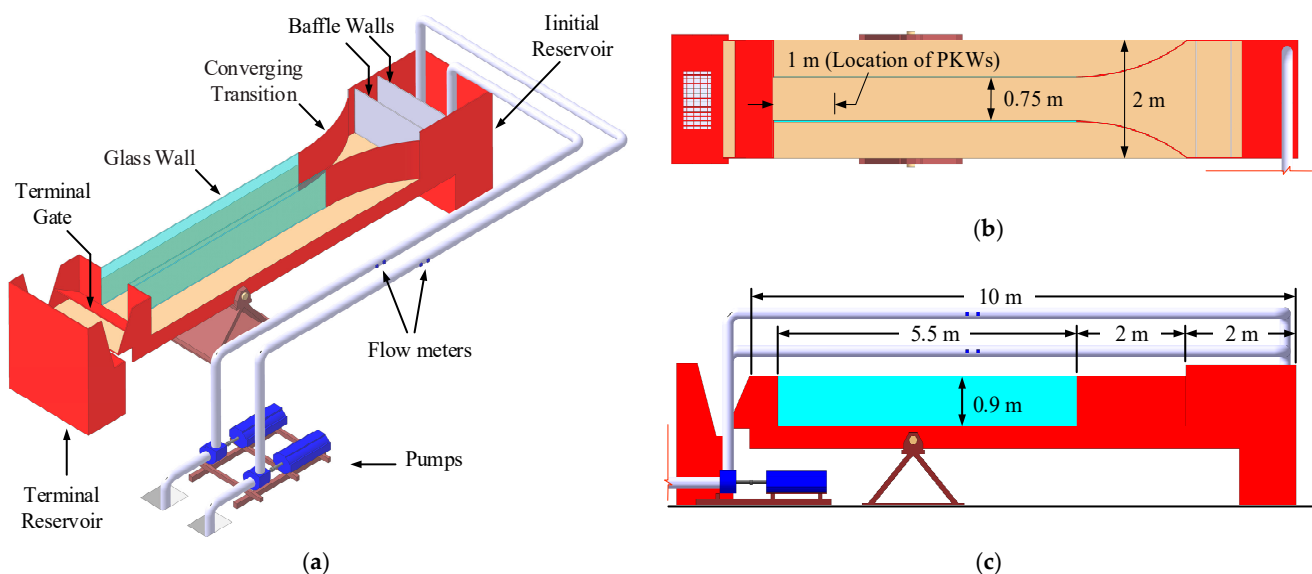

Figure 2. Overview of implemented test facilities: (**a**) the 3D view from downstream; (**b**) the plan view; (**c**) the side view.

The 3D rendering of the tested PKWs is presented in Figure 4. The base model was fabricated with $P = 325$ mm, $t = 20$ mm, and $N = 2$ (using High-Density Polyethylene (HDPE) sheeting and a computer numerically controlled (CNC) machine). The non-dimensional geometric parameters of this model were considered to be similar to the tested model by Anderson and Tullis (2013) [17], except for that the base model had a uniform short parapet wall (with the height of $P_p = 10$ mm) with a half-round crest shape (with the radius of $R_{crest} = t/2 = P_p = 10$ mm). The nine other models (Tri-B1 to Rec-B3 in Figure 4) were fabricated using a 3D printer having $P = 200$ mm, $t = 12$ mm, $N = 3$ and flat and quarter-round crest shapes for the normal and side walls ($R_{crest} = t = 12$ mm). Table 1

indicates the specifications of all of the tested weirs along with the measured parameters (denoted by the ■ symbol).
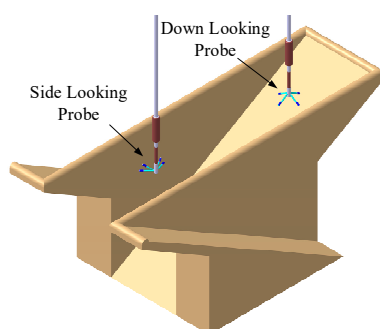
Figure 3. Velocity measurements near the vertical walls and sloped floors (upstream view, base model (weir height (*P*) = 325 mm)).
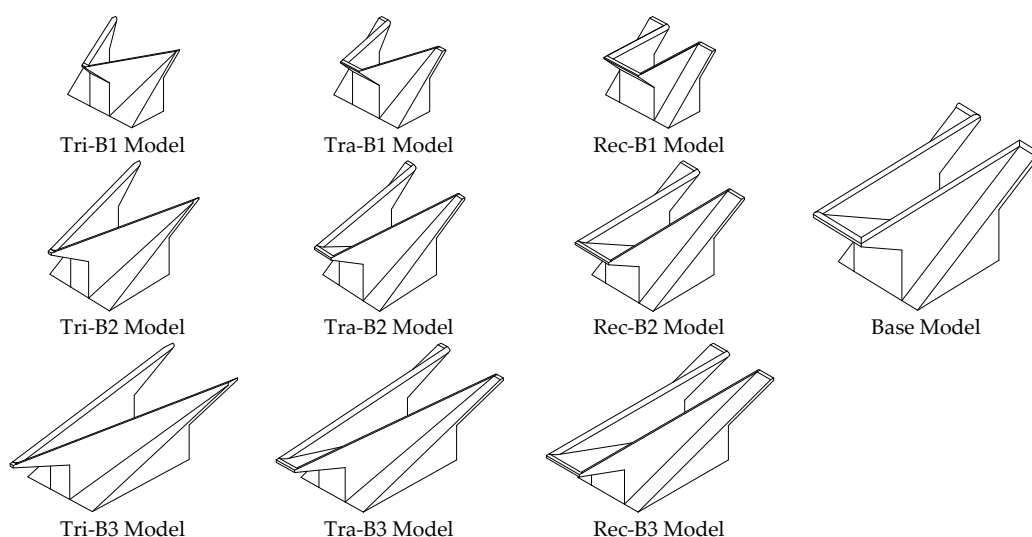
Figure 4. A Three-dimensional view of the tested models (1 key, downstream view).

**Table 1.** Different data measurements (denoted by the ■ Symbol) for PKW Models with various apex width ratios (A/w) and length magnification ratios (B/w).

Model	B/w	A/w	L (m)	α (°)	Inlet Keys		Outlet Keys			Head-Discharge Data
					Water Surface Profiles	Velocity Data	Nappe Aeration	Interference Length	Standing Wave Characteristics	
Base [a]	2.05	0.50	3.750	0	■	■	□	□	□	■
Tri-B1 [b]	1.00	0.00	1.613	26.6	■	■	■	■	□	■
Tra-B1	1.00	0.25	1.851	14.7	■	□	■	□	□	■
Rec-B1	1.00	0.50	2.178	0	■	□	■	■	□	■
Tri-B2	2.00	0.00	3.023	14.0	■	■	■	□	□	■
Tra-B2	2.00	0.25	3.327	7.3	■	□	■	□	■	■
Rec-B2	2.00	0.50	3.678	0	■	■	■	□	■	■
Tri-B3	3.00	0.00	4.491	9.5	■	□	■	■	□	■
Tra-B3	3.00	0.25	4.819	4.8	■	□	■	□	■	■
Rec-B3	3.00	0.50	5.178	0	■	□	■	■	■	■

[a] Specifications of the base model: $w/P_o = 1.19$, $B_i/B = B_o/B = 0.25$, $A/D = 1.25$, $t/P_o = 15.75$, $N = 2$, $S_o = 0$, and half-round crest shape [having $P = 325$ mm (including $P_p = 10$ mm)]. [b] Specifications of the models Tri-B1 to Rec-B3: $w/P = 1.25$, $B_i/B = B_o/B = 0.25$, $A/D = 1$, $t/P = 16.6$, $N = 3$, $S_o = 0$, and the quarter-round and flat crest shapes for side and normal walls, respectively [having $P = 200$ mm ($P_p = 0$)].

4. Results and Discussion

4.1. Flow Behavior in Inlet Keys

The complex flow structure around PKWs might be better understood by studying water surface profiles. The longitudinal profiles in the inlet key may have a dual behavior. As shown in Figure 5a, in the upstream part of the inlet key, the water surface drops due to the contraction of the subcritical flow (caused by the weir walls and upward floors). the supercritical inflow in the terminal portions then responds to the contraction as a slight rise in the water surface. From Figure 5a, the comparison of profiles in the inlet key and the sidewall centerlines indicates that the water surface decreases near the sidewalls due to the drawdown effects of the lateral spilling flow. Similar trends for the water surface profile were observed by Anderson and Tullis (2012) and Machiels (2012) [16,40].
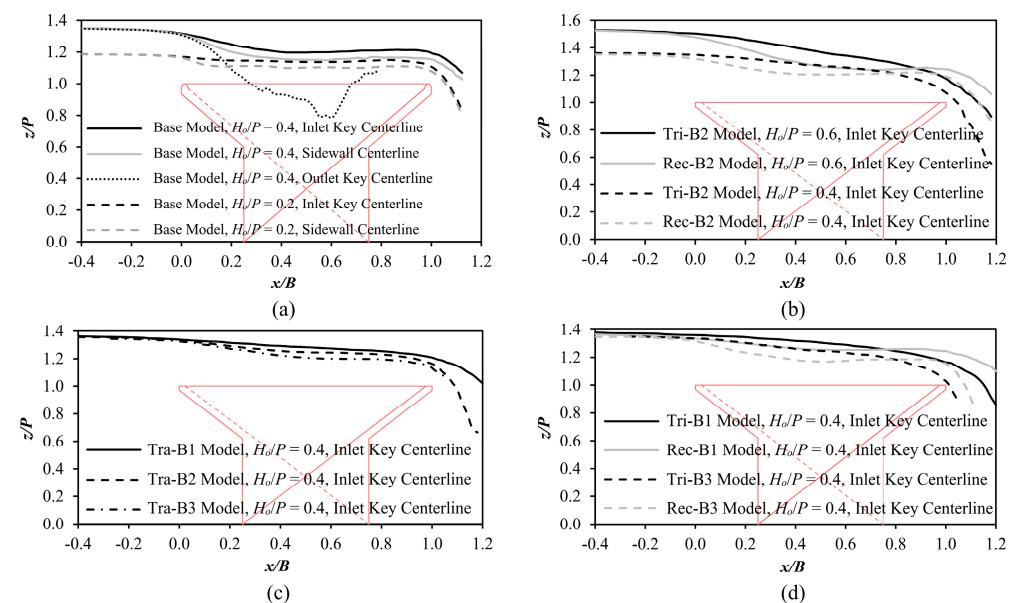

Figure 5. Water surface profiles in different models with various headwater ratios (H_o/P): (**a**) base model; (**b**) Tri-B2 and Rec-B2 models; (**c**) Tra-B1, Tra-B2, and Tra-B3 models; (**d**) Tri-B1, Rec-B1, Tri-B3, and Rec-B3 models.

From Figure 5b, the water surface drop in the inlet key is more significant in larger A/w values (especially in high head conditions). This is because the initial portion of the inlet key, through which the inflow enters into the weir, is wider in a triangular shape (shown in Figure 6); thus, the inflow contraction lessens. According to Figure 5c, a larger drop occurs for larger values due to having a narrower space between the weir walls. The interactions between the two parameters A/w and B/w in Figure 5d illustrate that the water surface drop occurring at higher values is more severe for a larger A/w.
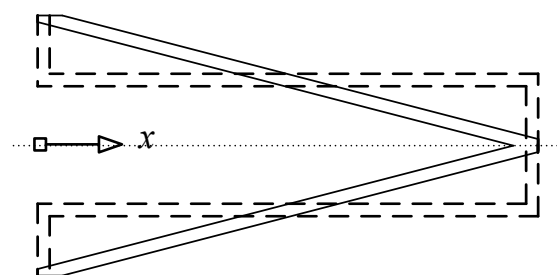

Figure 6. Comparison of the width of rectangular (A/w = 0.5) and triangular (A/w = 0) plan shapes.

Flow field around the PKWs was also studied to improve understanding of their hydrodynamics and flow mechanisms. Figure 7 shows the velocity profiles in the inlet key centerline of the base model (u = time-averaged velocity in x-direction; V = average cross-sectional velocity of approaching flow). As shown, the velocity profiles have a dual behavior that is similar to water surface profiles. When the flow enters the inlet key, the velocity increases in the streamwise direction due to the accelerating drawdown effects and the inflow contraction. However, the longitudinal velocity reduces in the inlet key terminal portions (higher x/B values) because of the sloped floor and the reduction in the inflow rates in the downstream direction as flow discharges into outlet keys. From Figure 7a, the flow velocity increases by an increase in H_o/P to pass a larger discharge over the weir. However, the dimensionless velocity (u/V) in Figure 7b is a decreasing function of H_o/P, which can be attributed to the large relative inlet key flow contraction and the associated head loss. The difference between the u/V profiles of the two different headwater ratios (H_o/P = 0.1 and 0.2) is at its maximum in the middle portions of the inlet key (x/B = 0.37), which is where the inflow contraction occurs. However, according to Figure 8, this difference is negligible for a triangular plan shape (Tri-B2 model), where the inflow contraction is not significant. From Figure 9, it can be found that u/V, and subsequently, the flow momentum in the streamwise direction can be enhanced by increasing A/w and B/w (more weir length).
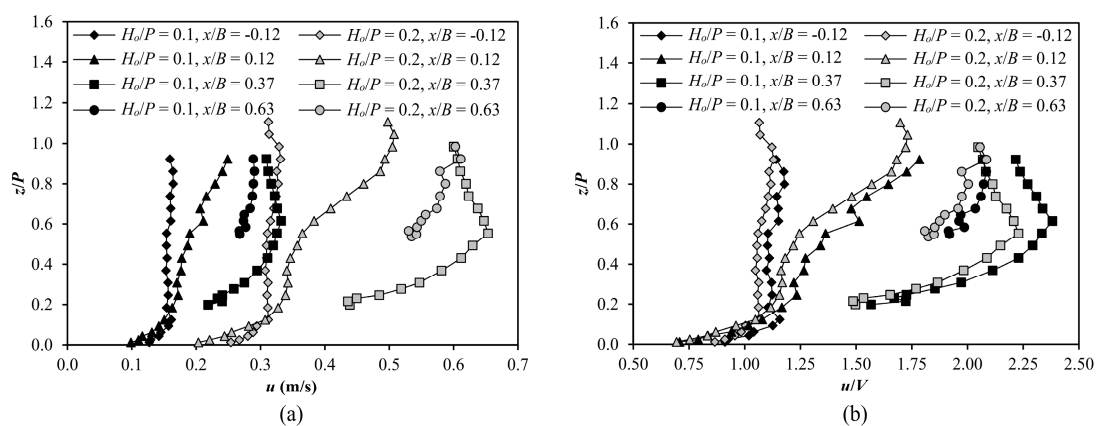
Figure 7. Velocity profiles in the inlet key centerline of the base model: (**a**) dimensional value; (**b**) dimensionless value. (V = 0.139 and 0.293 m/s for H_o/P = 0.1 and 0.2, respectively).
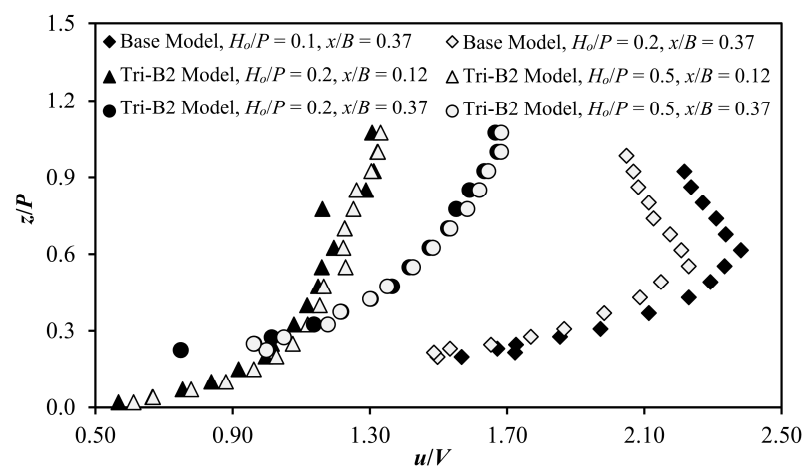
Figure 8. Dimensionless velocity profiles in inlet key centerlines (V = 0.140, 0.293, 0.197, and 0.454 m/s at the base model with H_o/P = 0.1 and 0.2 and the Tri-B2 model with H_o/P = 0.2 and 0.5, respectively).
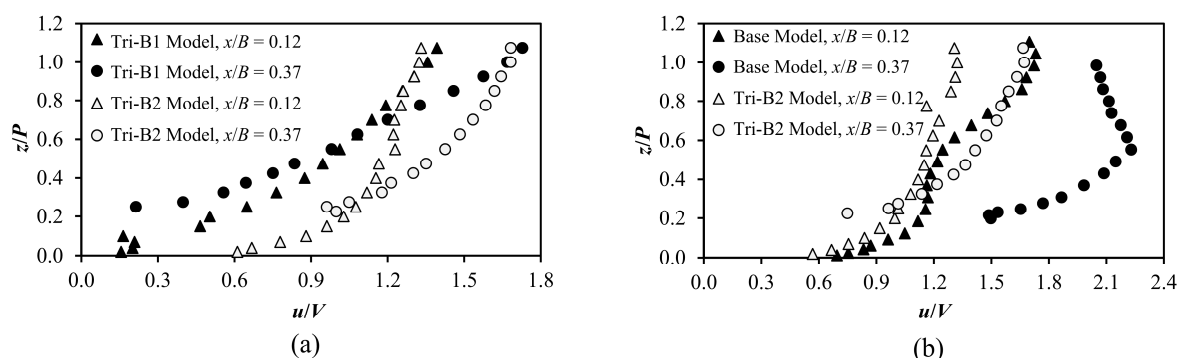
Figure 9. Dimensionless velocity profiles in the inlet key centerline: (**a**) $H_o/P = 0.5$ ($V = 0.337$ and 0.454 m/s at the Tri-B1 and Tri-B2 models, respectively); (**b**) $H_o/P = 0.2$ ($V = 0.293$ and 0.197 m/s at the base and Tri-B2 models, respectively).

A separation (or recirculation) zone was identified by Machiels et al. (2011) in the inlet keys of a rectangular PKW [31]. To determine its variations, the velocities were measured in different planes around different PKWs (P1 in Tri-B1, P1 in Tri-B2, and P1 and P4 in Rec-B2, as shown in Table 2). However, the collected data may not visualize the separation zone because of having a CC < 0.7 (probably due to the high level of flow unsteadiness and weir wall disruption in the transmission of acoustic waves). Nevertheless, from Figure 10, the high diffusion of the injected dye confirms the presence of the separation zone in the downstream section of a rectangular PKW. It may diminish at the smaller A/w values, where the sidewalls act as a nose to guide the inflow. In addition, the recirculation vortices may appear as some undulations on the water surface (not observed for smaller A/w and H_o/P values).

**Table 2.** Specifications of velocity measurement planes.

Model	Plane No.	Orientation	x/B	y/w	z/P	Node Numbers	Sketch
Base	P1	Horizontal	0.00–0.80	0.50–0.74	0.862	30	
	P2	Horizontal	0.00–0.80	0.50–0.74	0.954	30	
Tri-B1	P1	Horizontal	0.18–0.44	0.67–0.86	0.750	56	
Tri-B2	P1	Horizontal	0.18–0.44	0.61–0.87	0.750	68	
Rec-B2	P1	Horizontal	−0.05–0.65	0.55–0.70	0.750	120	
	P2	Horizontal	0.00–0.80	0.55–0.73	1.100	30	
	P3	Horizontal	0.00–0.80	0.55–0.73	1.200	30	
	P4	Vertical	0.15–0.45	0.294	0.55–0.85	128	
	P5	Vertical	0.15–0.25	0.726	1.13–1.28	77	
	P6	Vertical	0.000	0.78–0.94	1.13–1.33	81	
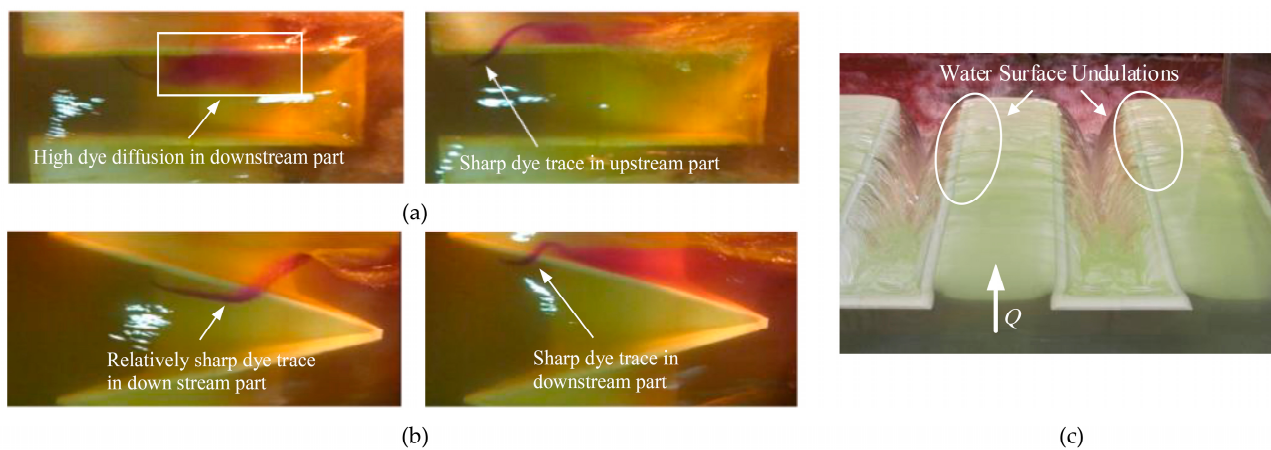
Figure 10. Experimental observations: (**a**) dye trace in Rec-B2 ($H_o/P = 0.65$, left-to-right flow direction); (**b**) dye trace in Tri-B2 ($H_o/P = 0.65$); (**c**) water surface undulations in Rec-B3 ($H_o/P = 0.147$).

Beyond the PKW structure, the ADV data may have a high quality (e.g., CC > 0.9 for planes P5 and P6 in the Rec-B2 model, as shown in Table 2). Figure 11 presents the velocity vectors in the vicinity of the crest of the Rec-B2 and base models. By increasing H_o/P, the accelerated inflow obeys the general channel flow direction more. However, at a smaller distance from the crest, the inflow more tends to stay at the sidewalls. The contours of the angle between the velocity vectors and the weir sidewall (Θ) are presented in Figure 12 for the two mentioned rectangular models ($\alpha = 0°$). As shown, Θ reduces by increasing H_o/P and by moving away from the crest in both the vertical and horizontal directions (less weir effects on the flow). Figure 13 shows Θ variations along the sidewall centerline of the triangular and rectangular PKWs. Generally, Θ increases with x/B in the sidewall initial portion; however, it shows a reverse trend in its terminal portion (due to the increased flow acceleration in the streamwise direction). In addition, since α has a significant contribution in Θ, a triangular plan has a larger Θ compared to a rectangular one (closer to the ideal condition; $\Theta = 90°$). Moreover, Θ increases by decreasing B/w because a lower flow momentum allows the inflow to turn more readily and spill over sidewalls (refer to Figure 9a).
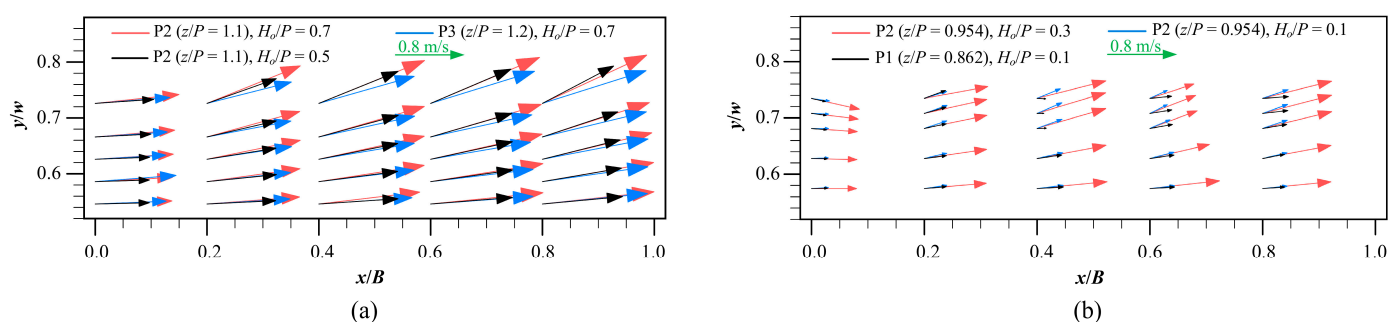
Figure 11. Velocity vectors in (**a**) Rec-B2 model; (**b**) base model.

The discharge locally changes along the crest of a PKW (unit discharge = q = magnitude of velocity component normal to the wall × flow depth). From Figure 5a, the uniform flow depth over the upstream normal wall (the same water surface levels at $x/B \approx 0$ for the sidewall and outlet key centerlines) is clearly larger than that over the side walls, and their difference progressively enlarges with an increase in H_o/P. Thus, higher values of u compared to v (which are the normal velocity components on the normal and side walls of a rectangular PKW, respectively) in Figure 14 reveal that the unit discharge on the upstream normal wall (= $u \times h$) can be several times larger than that of the sidewall (= $v \times h$) in

such a relatively high H_o/P. It is worth noting that the low-quality velocity data in the downstream section prevented the determination of q on the whole PKW crest. In addition, despite a lower q, the total discharge over the sidewalls is larger than that of the normal walls because the sidewalls are usually much longer than the normal walls.

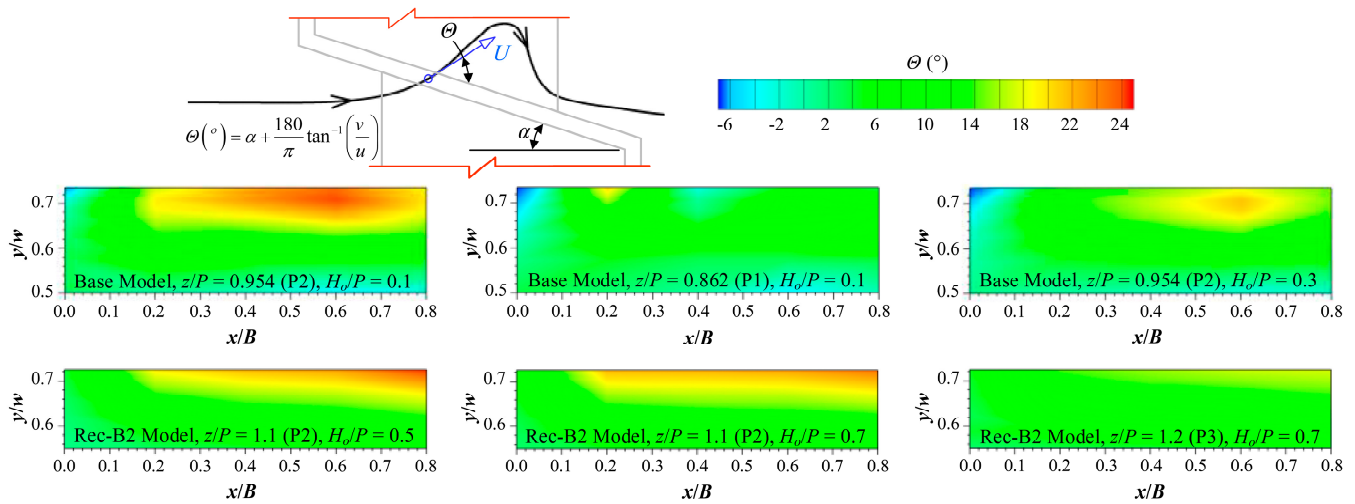**Figure 12.** Contours of Θ for the base model (**upper** figures) and the Rec-B2 model (**lower** figures).
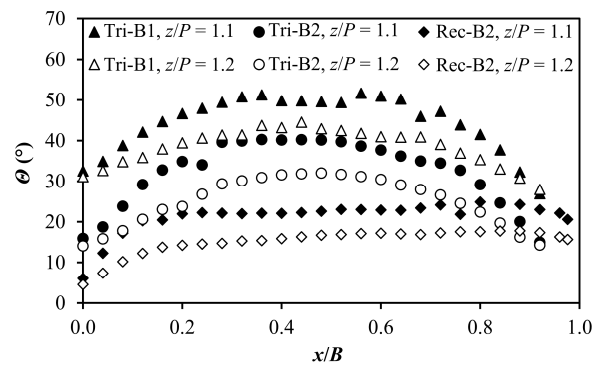

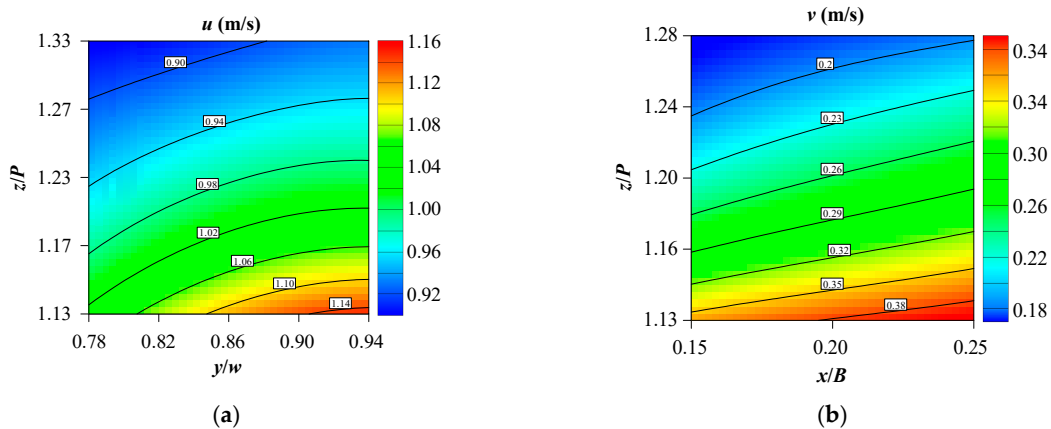**Figure 13.** Variations of Θ along the PKW sidewall centerline ($H_o/P = 0.7$).

Figure 14. Velocity contours in Rec-B2 ($H_o/P = 0.7$): (**a**) u-component above the upstream normal wall (P6, upstream view); (**b**) v-component above the side wall (P5, side view).

4.2. Flow Behavior in Outlet Keys

The flow mechanisms in outlet keys are also mapped by studying the nappe aeration and interference. By increasing H_o/P, the nappe aeration regime generally transforms from a clinging regime to an aerated regime, then transforms to partially aerated regime, and finally, it transforms to drowned regime [40,42]. According to experimental observations, in the clinging regime, the nappe adheres to the downstream face of the sidewalls (not necessarily the overhangs) due to the subatmospheric pressures on them [11]. By increasing the head, the flow momentum separates the nappe from the weir wall (aerated regime). In the partially aerated regime, one or more unstable air cavities (in size and location) move along the weir sidewalls, leading to an uncertainty in the determination of the PKW discharge capacity (addressed in the next section). Finally, in the drowned regime, the thick overflow nappe prevents air pocket formation.

Figure 15 indicates that $H_o/P \approx 0.1$ can be considered as an approximate threshold for the aerated regime of the PKWs (which may be sensitive to weir scale and crest shape). In addition, by increasing A/w (changing the plan shape from triangular to trapezoidal and then to rectangular again), the drowned regime starts with higher H_o/P values. This is because the sharper apex corners (smaller values of α) facilitate nappe splitting and aeration. However, at higher B/w and A/w values, the nappe aeration regime is less impacted by the weir geometry. It is also shown that for lower values of B/w, the drowned regime occurs at smaller headwater ratios because these geometries are more susceptible to the nappe interference (discussed later in the current section).
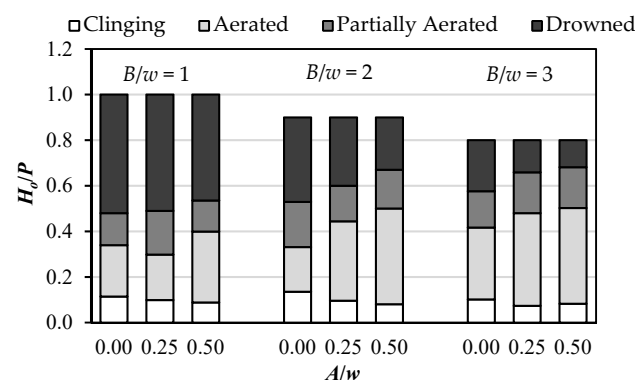

Figure 15. Variations of flow aeration regime with H_o/P, A/w, and B/w.

According to Figure 15, when B/w = 3 and A/w = 0, the thresholds of the partially aerated and drowned regimes are H_o/P = 0.42 and 0.58, respectively. The corresponding values were reported as 0.29 and 0.39 by Crookston and Tullis (2013) for a labyrinth weir with relatively similar dimensionless parameters (B/w = 2.8 and A/w = 0.06) [42]. Therefore, it can be presumed that due to the presence of the inlet key (or downstream) overhangs, a PKW experiences better aeration conditions compared to a labyrinth weir. Studying trapezoidal PKWs with small overhangs ($B_i/B = B_o/B$ = 0.1), Mehboudi et al. (2017) reported values of H_o/P = 0.18 and 0.35, as the general thresholds of the partially aerated and drowned regimes for all of their 36 models were in the ranges of $1.22 \leq B/w \leq 2.86$ and $0.19 \leq A/w \leq 0.42$ [44]. Although theses researchers did not report the variations of nappe aeration with PKW geometry, their general thresholds are smaller than the corresponding headwater ratios for the whole range of the present study ($1 \leq B/w \leq 3$ and $0 \leq A/w \leq 0.5$), as shown in Figure 15. This may be due to the larger overhangs of the current study models ($B_i/B = B_o/B$ = 0.25). Again, it worth noting that the scale effects may significantly affect the nappe behavior, especially for the above-mentioned H_o/P threshold values for H_o/P.

Nappe interference also occurs in PKW outlet keys including either a region of local submergence, a standing wave, or both [40,41]. As shown in Figure 16, considering the intersection of the weir crest elevation with the water surface profile, the parameter of

interference length (B_{int}) as the summation of the local submergence length (B_{sub}) and the standing wave length (B_{wav}) are used to characterize the extent of nappe interference (measured on the centerline of outlet keys). It is notable that a standing wave is not formed in a triangular PKW (Figure 16c), most likely due to the large width of the downstream portion of outlet keys. In addition, the flow features in the outlet keys are often dynamic and highly unstable, especially in high head conditions (time-mean values of the measured parameters were recorded for further analyses).
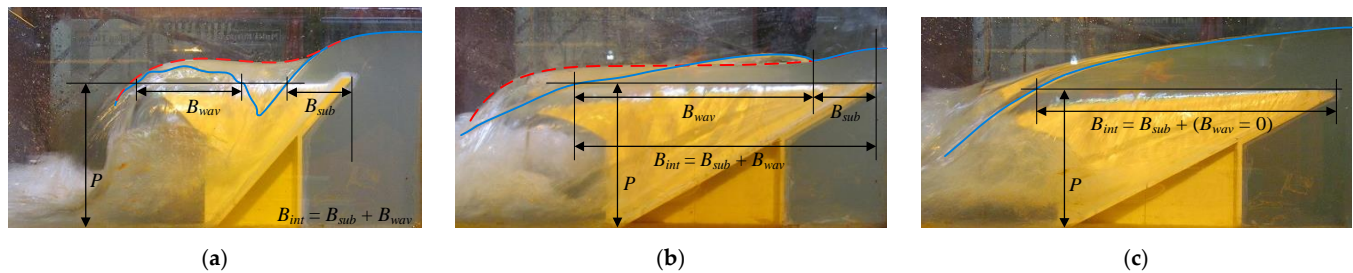
Figure 16. Nappe interference characteristics: (**a**) Rec-B1, Ho/P = 0.30; (**b**) Tra-B2, Ho/P = 0.30; (**c**) Tri-B2, Ho/P = 0.49; (————— water surface profile in outlet key centerline; --------- water surface profile in inlet key centerline).

The variations of B_{int}/B and B_{sub}/B are presented in Figure 17 (B_{wav}/B can be also determined by subtracting these two parameters). As expected, both parameters generally increase with an increase in H_o/P. However, their increasing trends may stop (or reverse) with smaller values of A/w and B/w when $0.3 < H_o/P < 0.6$. This drop may be due to the aeration regime transition (Figure 15). By starting the partially aerated regime, which results in a reduction in the nappe aeration, the nappe appears to become closer to the weir sidewalls. Thus, the nappe interference reduces. It should be noted that the mentioned drop diminishes with larger values of B/w and A/w (minor effects of aeration regime transition). The jump noted in the B_{int}/B curve of the Rec-B1 model is because in the low head conditions, the standing wave is lower than the weir crest ($B_{wav} = 0$), while it exceeds the crest in higher flow heads (B_{wav} is also added to B_{int}).
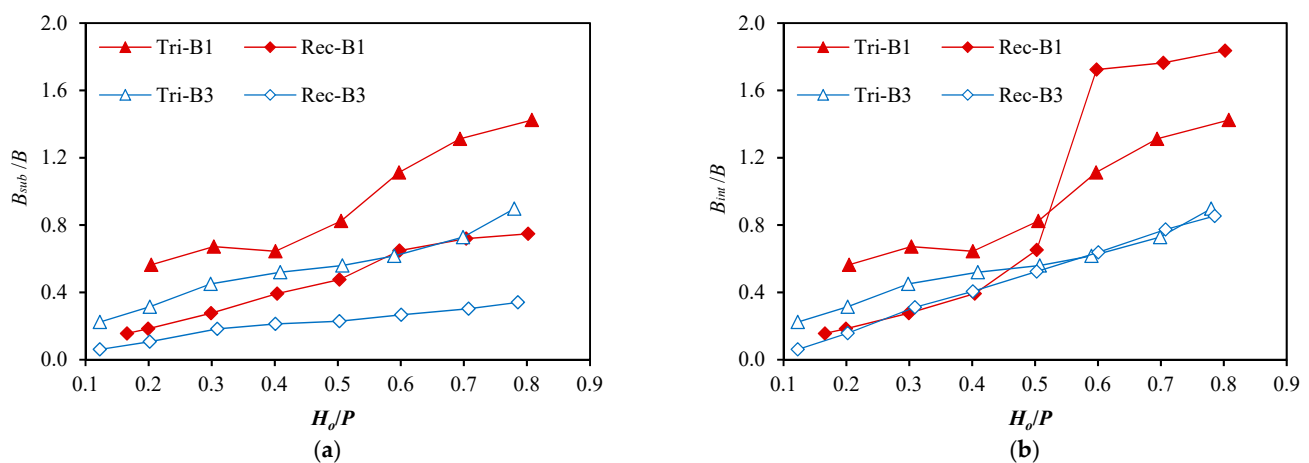
Figure 17. Variations of (**a**) local submergence length and (**b**) interference length.

According to Figure 17a, the local submergence length of triangular PKWs is larger than that of the rectangular ones. This is because the initial part of the outlet key (susceptible location for local submergence occurrence) is narrower in a triangular PKW (Figure 6). This point also justifies why in the interference lengths of triangular PKWs Figure 17b are larger than those of rectangular PKWs in low head conditions, where the overflow is concentrated on the initial portions of the PKWs. However, a triangular shape may have a smaller B_{int}/B at higher H_o/P values (more pronounced in lower B/w values corresponding to larger

sidewall angles). This is because in high head conditions, the overflow concentrates on the terminal portions of the PKWs, where a triangular shape has larger discharge area. From Figure 17, it can also be seen that although B_{sub} and B_{int} may increase due to an increase in B (larger discharge capacity), their growth rates are not as fast as that of B. As a result, the dimensionless parameters B_{sub}/B and B_{int}/B are decreasing functions of B/w. This result is in agreement with the performance of trapezoidal labyrinth weirs [41].

4.3. Discharge Coefficient and Efficiency

The variations of the PKW discharge coefficient are presented and analyzed in this section. According to Figure 18, C_d is an increasing function of H_o/P in very low head conditions ($H_o/P < 0.1$ corresponding to the clinging regime in Figure 15). In this regime, an increase in H_o/P intensifies the subatmospheric pressures under the nappe and consequently leads to an increase in C_d. However, the increasing trend of C_d stops at the beginning of the aerated regime. Its monotonic decreasing trend with H_o/P may be due to the local submergence enlargement in the outlet keys (Figure 17) and the inflow contraction in the inlet keys (shown as water surface drop in Figure 5), which reduce the effective crest length and weakens the performance of the sidewalls (lower Θ values in Figure 12).
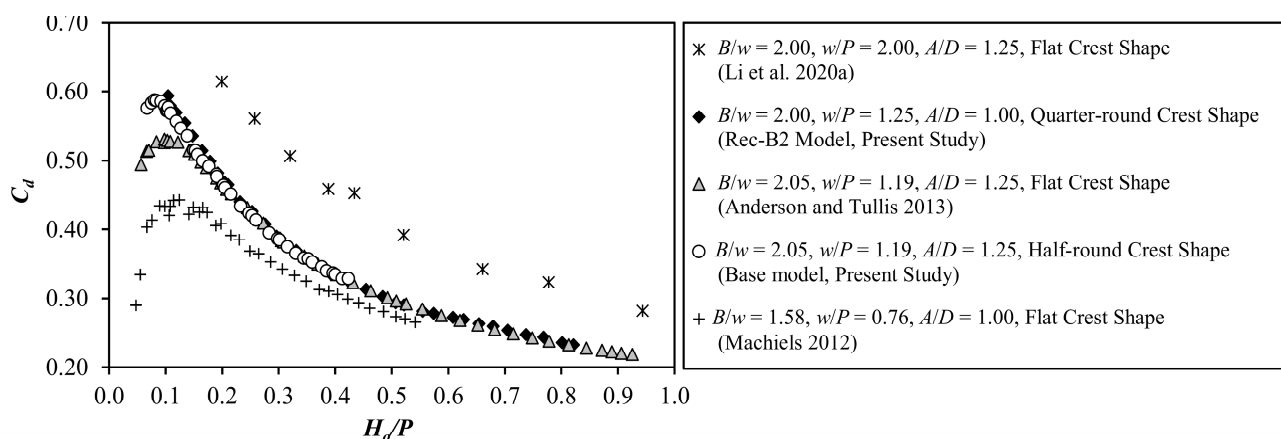

Figure 18. Comparison between the results of the present and previous studies (all geometries have a rectangular plan shape and identical overhang ratio of $B_i/B = B_o/B = 0.25$).

From Figure 18, the comparison between the base model (from the present study) and the studied geometry by Anderson and Tullis (2013) [17] demonstrates that a half-round crest shape is more efficient than a flat one in low head conditions ($\sim H_o/P < 0.15$). Based on the results of Cicero and Delisle (2013) [26], the gain of a half-round crest shape is limited to ~20 percent, and it diminishes by increasing the H_o/P value (which can be confirmed by the mentioned comparison). In addition, the base and the Rec-B2 models from the present study show similar performance since the difference in A/D happens to be countered by the w/P difference. Based on the results of previous studies [17,25,27], the C_d of a rectangular PKW increases by ~10% by increasing the inlet-to-outlet width ratio from $A/D = 1$ to ~1.25, leading to a reduction in the inlet key velocity. On the other hand, C_d decreases in lower w/P values due to an increase in the nappe interference ratio [53], which can be seen by comparing the data of Anderson and Tullis (2013) and Li et al. (2020) [17,32]. This point can be validated by comparing the Rec-B2 model to the mentioned geometry of Machiels (2012) [40], which has a smaller C_d regardless of having a lower B/w value (the decreasing trend of C_d with B/w is subsequently presented in the current section).

Besides the variations in the apex width, the change in the sidewall angle should also be considered when analyzing the dual effects of A/w on C_d. Figure 6 indicates that for a given width, an increase in A/w enlarges the apex width with a normal orientation to the approaching flow (improving factor for C_d), while this change aligns the weir sidewalls to the flow (worsening factor for C_d). Thus, there is a balance between the performance of

normal wall and sidewall crests. According to Figure 19, at low H_o/P values, a trapezoidal PKW ($A/w = 0.25$) has higher C_d compared to a triangular one ($A/w = 0$). This is because the trapezoidal plan shape has larger apexes (as the best-orientated weir parts to the approaching flow), while having a lower sidewall angle does not limit its performance in low head conditions. However, the C_d of a triangular PKW overtakes that of the other shapes in higher headwater ratios ($H_o/P > 0.4$). In these conditions, the accelerated flow in the stream-wise direction cannot quickly turn and pass over the PKW sidewalls. Thus, an increase in A/w (leading to a higher α) can improve the sidewall orientation to the approaching flow (higher Θ values in Figure 13) and increases its contribution in the discharging flow. Another reason for the C_d reduction in higher A/w values may be the separation zone enlargement in the inlet keys (Figure 10), leading to a reduction in the effective flow area.
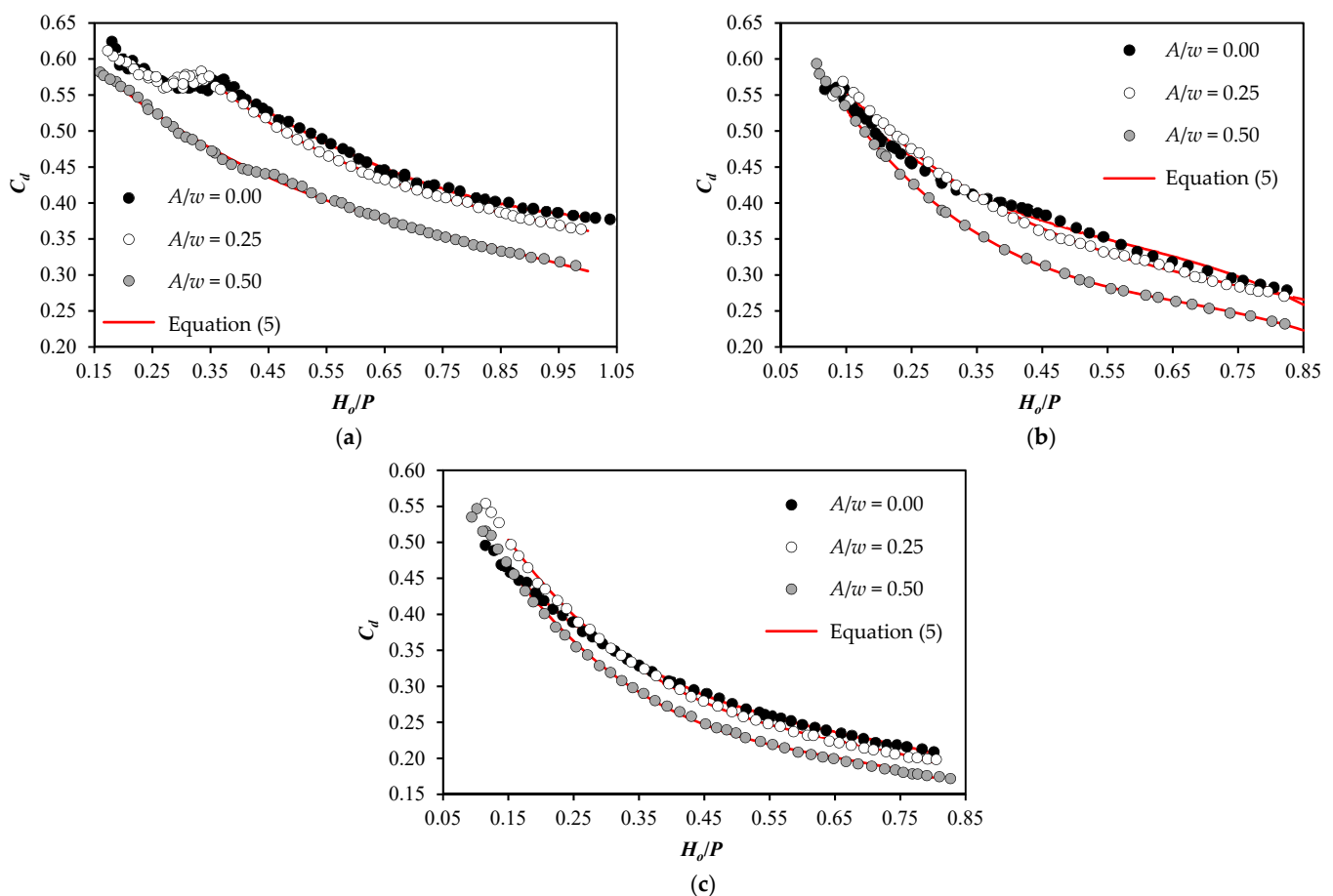
Figure 19. Variations of the discharge coefficient (C_d): (**a**) $B/w = 1$; (**b**) $B/w = 2$; (**c**) $B/w = 3$.

Since the flow features in the outlet keys are improved by increasing B/w (smaller values of B_{sub}/B and B_{int}/B in Figure 17), the decreasing trend of C_d with B/w is related to the inlet key features, including the increased inflow contraction (larger water surface drop in Figure 5d), the enhanced longitudinal flow inertia (larger u/V values in Figure 9a), and subsequently, the weaker performance of the sidewalls (smaller Θ values in Figure 13). According to Figure 19, for the low values of A/w and B/w, there is a jump in C_d when $0.3 < H_o/P < 0.4$. This is attributed to the transition from an aerated to a partially aerated regime (smaller air pocket under the nappe leading to a smaller nappe interference). However, this jump diminishes the larger values of B/w and A/w that correspond to the minor effects of the aeration regime transition.

Equation (5) is selected to describe the discharge coefficient of the PKWs [5], where a_1 to a_4 are empirical coefficients (obtained using the least-squares method). These coef-

ficients along with the coefficient of determination (R^2) and the average and maximum errors ($Error_{ave}$ and $Error_{max}$) are presented in Table 3. The minimum R^2 of 0.992 and the maximum error of 2.6% confirm that there is a strong agreement between the measured and calculated C_d values of the tested models (plotted on Figure 19).

$$C_d = a_1 \left(\frac{H_o}{P} \right)^3 + a_2 \left(\frac{H_o}{P} \right)^2 + a_3 \left(\frac{H_o}{P} \right) + a_4 \tag{5}$$

Table 3. Empirical constants of the discharge coefficient equation.

Model	B/w	A/w	Ho/P	a_1	a_2	a_3	a_4	R^2	$Error_{ave}$ (%)	$Error_{max}$ (%)
Base	2.05	0.50	0.10-0.45	−0.1648	1.6960	−1.6280	0.7253	0.9994	0.3	0.8
Tri-B1	1.00	0.00	0.35-1.00	−0.0213	0.4052	−0.8165	0.8137	0.9975	0.5	1.3
Tra-B1	1.00	0.25	0.35-1.00	−0.4118	1.2077	−1.3452	0.9106	0.9991	0.2	0.8
Rec-B1	1.00	0.50	0.20-1.00	−0.3388	0.8687	−0.9368	0.7123	0.9982	0.6	1.8
Tri-B2	2.00	0.00	0.15-0.85	−1.1316	1.9932	−1.4044	0.7073	0.9936	1.3	2.3
Tra-B2	2.00	0.25	0.15-0.85	−0.6128	1.4386	−1.3158	0.7214	0.9966	0.8	1.8
Rec-B2	2.00	0.50	0.15-0.85	−1.2809	2.5798	−1.9019	0.7625	0.9998	0.3	0.9
Tri-B3	3.00	0.00	0.15-0.80	−0.6919	1.5103	−1.2862	0.6248	0.9996	0.4	1.4
Tra-B3	3.00	0.25	0.15-0.80	−1.2469	2.5371	−1.9093	0.7369	0.9993	0.7	2.0
Rec-B3	3.00	0.50	0.15-0.80	−1.3602	2.7110	−1.9634	0.7054	0.9989	0.9	1.7

The discharge efficiency of PKWs ($\varepsilon = C_d \times L/W$) is also presented and analyzed [5]. According to Figure 20, while ε has a decreasing trend with H_o/P, it can be improved by increasing B/w and A/w; thus, the decrease in C_d can be restituted by increasing the weir length. However, Figure 21 demonstrates that the efficiency gains of increasing B/w and A/w diminish at higher H_o/P values (more intense nappe interference). For example, by increasing the magnification ratio from $B/w = 1$ to 3, the efficiency can be improved up to 80% when $H_o/P = 0.2$, while the gains are limited to ~25% in high head conditions. It is also shown in Figure 21a that the increase in efficiency caused by increasing B/w is more noticeable for lower values of A/w (lower inflow contraction). According to Figure 21b, although the efficiency a rectangular PKW is the most for $H_o/P > 0.5$ and $B/w = 1$, a trapezoidal PKW has the most-efficient plan shape when $H_o/P > 0.25$ and $B/w \geq 2$ ([corresponding to the majority of PKW prototypes across the world [56]).]. In addition, Table 4 shows that the body volume (C) of a trapezoidal shape is less than that of a rectangular one. Thus, assuming that the PKW global cost is proportional to its body volume [57], the trapezoidal shape may be selected as the optimal one. For a specific project, this point can be confirmed after a detailed cost estimation on the different elements of PKWs (i.e., weir foundation, wedge shape base, overhang, and vertical wall).
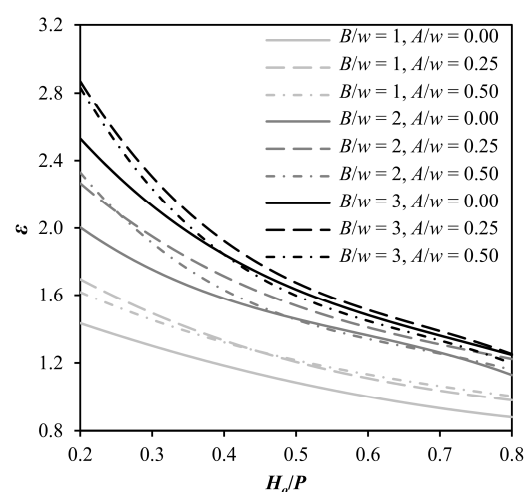

Figure 20. Efficiency curves.
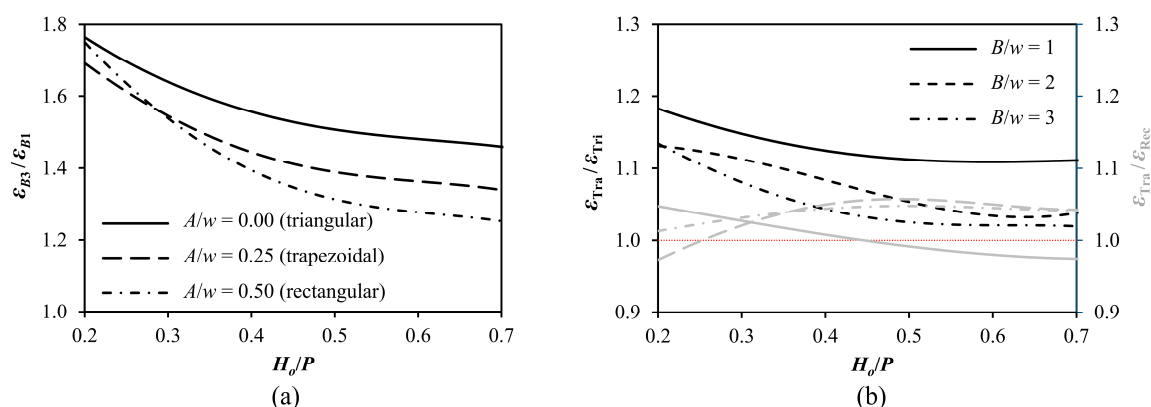
Figure 21. Relative efficiency of PKWs versus: (**a**) H_o/P and A/w (subscripts of $B3$ and $B1$ respectively refer to $B/w = 3$ and 1), respectively;); (**b**) H_o/P and B/w (subscripts of Tri, Tra, and Rec respectively refer to $A/w = 0$, 0.25, and 0.5, respectively).

Table 4. Volume of PKW bodies (C) in the experimental scale with three keys.

B/w	$C \times 10^3$ (m^3)		
	$A/w = 0.00$	$A/w = 0.25$	$A/w = 0.50$
1	9.3	10.3	11.2
2	18.6	20.1	21.7
3	27.8	30.0	32.2

From Table 4, C has almost a constant growth rate with respect to B/w ([i.e., the body volume of a PKW having $B/w = n$ is almost n times that of a PKW with $B/w = 1$).]. However, according to Figure 22, the discharge growth rate does not have a linear trend, and it slows down by increasing B/w. Therefore, there is no optimal solution for B/w from the hydraulic point of view, and it can be determined after considering site-specific constraints and costs.
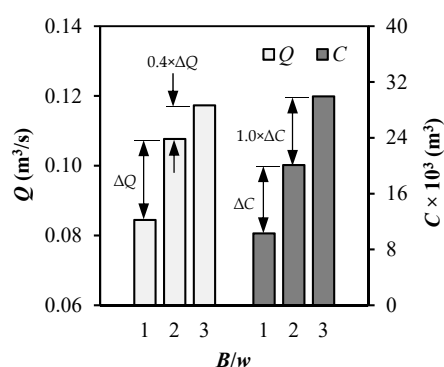
Figure 22. PKW discharge (Q) and body volume (C) versus B/w: ($H_o/P = 0.5$, $A/w = 0.25$).

5. Conclusions

This paper studies the flow behavior around PKWs with different plan shapes in the wide ranges of H_o/P and B/w. The results led to the following conclusions:

- The water surface drop and recirculation zone, occurring in PKW inlet keys respectively due to the inflow contraction and the sharp-corner entrance, are more severe at higher values of H_o/P, B/w, and A/w. At higher H_o/P values and at larger distances from the weir crest, the passing flow is less affected by the PKW structure. However, by reducing the weir length and apex width, the weir structure effects on the passing flow retrieve;

- While the aeration regimes vary with the weir geometry, $H_o/P = 0.1$ can be considered as the general threshold for the aerated regime of the tested PKWs (sensitive to weir scale and crest shape). In addition, by increasing B/w and A/w, the flow aeration regimes extend to higher H_o/P values. By comparing the present study and previous studies [42], a PKW has better aeration conditions compared to a labyrinth weir;
- The parameter B_{sub}/B increases in lower A/w values. Although the standing wave is not formed in a triangular PKW, its B_{int}/B is larger than that of a rectangular one in low head conditions ($H_o/P < 0.5$). However, a reverse trend may happen in high head conditions (more pronounced in lower values of B/w). It was shown that the parameters B_{sub}/B and B_{int}/B have a decreasing and increasing trend with respect to B/w and H_o/P, respectively;
- Although the discharge coefficient has a certain decreasing trend with respect to H_o/P and B/w, it shows a dual trend with the plan shape. Compared to a triangular shape, the higher C_d of a trapezoidal PKW at $H_o/P < 0.4$ implies that C_d may have an increasing trend with respect to A/w in low head conditions (more data on $H_o/P < 0.15$ are needed to also include a rectangular shape in this conjecture and fully confirm it). However, it has a decreasing trend with the apex width ratio of $H_o/P > 0.4$. According to the obtained results, PKW efficiency gains monotonically diminish by increasing H_o/P. For example, by changing $H_o/P = 0.2$ to 0.7, the benefits of increasing the magnification ratio from $B/w = 1$ to 3 reduces to less than a third (around 25% gain in discharge capacity);
- While the rectangular plan shape is traditionally considered in PKW prototypes and scientific models, its efficiency is the most only for low-length PKWs ($B/w = 1$) under high head conditions ($H_o/P > 0.5$). By assuming that the cost of PKWs is proportional to their body volume, a trapezoidal shape can be selected as the optimal one. Compared to a rectangular shape, a trapezoidal PKW provides a higher discharge efficiency (~5%) with a smaller body volume (~7%) in the broad ranges of $H_o/P > 0.25$ and $B/w \geq 2$, which correspond to the majority of worldwide prototypes. A detailed cost estimation on the different elements of PKWs is needed to confirm this result for a specific project.

Author Contributions: Y.S., methodology, investigation, formal analysis, writing—original draft; H.T.-D., formal analysis, writing—review and editing, supervision; M.G., methodology, resources, writing—review and editing, supervision; M.M., formal analysis, writing—review and editing; R.Z., methodology, investigation. All authors have read and agreed to the published version of the manuscript.

Institutional Review Board Statement: Not applicable.

Informed Consent Statement: Not applicable.

Data Availability Statement: The data presented in this study are available upon request from the corresponding author.

Conflicts of Interest: The authors declare no conflict of interest.

Notations

The following symbols are used in this paper.

A	inlet key (or downstream) apex width
B	weir length in streamwise direction
B_b	footprint length
B_i	inlet key (or downstream) overhang length
B_{int}	interference length
B_o	outlet key (or upstream) overhang length
B_{sub}	local submergence length
B_{wav}	standing wave length

C	weir body volume
CC	correlation coefficient for velocity data measurements
C_d	discharge coefficient
D	outlet key (or upstream) apex width
d	flow depth
g	acceleration due to gravity
h	approach flow depth over the weir
H_o	total upstream head
L	total length of PKW
L_{key}	length of a single key
N	number of keys
P	weir heigh
Q	weir discharge
q	unit discharge
R	Reynolds number
R_{crest}	radius of rounded crest
S_e	crest shape representative
SNR	signal-to-noise ratio
S_o	longitudinal bed slope
t	weir wall thickness
U	Velocity vector
u, v	time-averaged velocity in the respective x and y-direction
V	average cross-sectional velocity of approaching flow
W	weir (or channel) width
W	Weber number
w	cycle width
x, y, z	longitudinal, transverse, and vertical directions, respectively
α	sidewall angle
ε	discharge efficiency
μ	dynamic viscosity
ρ	fluid density
σ	surface tension
Θ	angle between velocity vectors and weir sidewall

References

1. Fowler, H.; Wilby, R. Detecting changes in seasonal precipitation extremes using regional climate model projections: Implications for managing fluvial flood risk. *Water Resour. Res.* **2010**, *46*, W03525. [CrossRef]
2. Suprapto, M. Increase spillway capacity using Labyrinth Weir. *Procedia Eng.* **2013**, *54*, 440–446. [CrossRef]
3. Schleiss, A.J. From labyrinth to piano key weirs: A historical review. In *Labyrinth and Piano Key Weirs—PKW 2011*; CRC press: Liège, Belgium, 2011; pp. 3–15.
4. Petley, D. Edenville Dam: A Major Dam Vollapse in Michigan. Available online: https://blogs.agu.org/landslideblog/2020/05/20/edenville-dam-1/ (accessed on 20 May 2020).
5. Crookston, B.; Tullis, B. Hydraulic design and analysis of labyrinth weirs. I: Discharge relationships. *J. Irrig. Drain. Eng.* **2013**, *139*, 363–370.
6. Tiwari, H.; Sharma, N. Developments to improve hydraulic competence of spillways. *Aquat. Procedia* **2015**, *4*, 841–846. [CrossRef]
7. Savage, B.M.; Brenchley, S. Fish passage using broad-crested labyrinth weirs for low-head dams. *Int. J. River Basin Manag.* **2013**, *11*, 277–286. [CrossRef]
8. Azimi, A.H.; Hakim, S.S. Hydraulics of flow over rectangular labyrinth weirs. *Irrig. Sci.* **2019**, *37*, 183–193. [CrossRef]
9. Sangsefidi, Y.; MacVicar, B.; Ghodsian, M.; Mehraein, M.; Torabi, M.; Savage, B.M. Evaluation of flow characteristics in labyrinth weirs using response surface methodology. *Flow Meas. Instrum.* **2019**, *69*, 101617. [CrossRef]
10. Carollo, F.G.; Ferro, V.; Pampalone, V. Testing the outflow process over a triangular labyrinth weir. *J. Irrig. Drain. Eng.* **2017**, *143*, 06017007. [CrossRef]
11. Bilhan, O.; Aydin, M.C.; Emiroglu, M.E.; Miller, C.J. Experimental and CFD analysis of circular labyrinth weirs. *J. Irrig. Drain. Eng.* **2018**, *144*, 04018007. [CrossRef]
12. Tajari, M.; Dehghani, A.A.; Meftah Halaghi, M. Semi-analytical solution and numerical simulation of water surface profile along duckbill weir. *ISH J. Hydraul. Eng.* **2018**, *27*, 65–72. [CrossRef]
13. Sangsefidi, Y.; Mehraein, M.; Ghodsian, M.; Motalebizadeh, M.R. Evaluation and analysis of flow over arced weirs using traditional and response surface methodologies. *J. Hydraul. Eng.* **2017**, *143*, 04017048. [CrossRef]

14. Crookston, B.M.; Erpicum, S.; Tullis, B.P.; Laugier, F. Hydraulics of Labyrinth and Piano Key Weirs: 100 Years of Prototype Structures, Advancements, and Future Research Needs. *J. Hydraul. Eng.* **2019**, *145*, 02519004. [CrossRef]

15. Lempérière, F.; Ouamane, A. The Piano Keys weir: A new cost-effective solution for spillways. *Int. J. Hydropower Dams* **2003**, *10*, 144–149.

16. Anderson, R.; Tullis, B. Comparison of piano key and rectangular labyrinth weir hydraulics. *J. Hydraul. Eng.* **2012**, *138*, 358–361. [CrossRef]

17. Anderson, R.; Tullis, B. Piano key weir hydraulics and labyrinth weir comparison. *J. Irrig. Drain. Eng.* **2013**, *139*, 246–253. [CrossRef]

18. Laugier, F.; Vermeulen, J.; Blancher, B. Overview of design and construction of 11 piano key weirs spillways developed in France by EDF from 2003 to 2016. In *Labyrinth and Piano Key Weirs III—PKW 2017*; CRC Press: Qui Nhơn, Vietnam, 2017; pp. 37–51.

19. Erpicum, S.; Laugier, F.; Boillat, J.-L.; Pirotton, M.; Reverchon, B.; Schleiss, A. *Labyrinth and Piano Key Weirs—PKW 2011*; CRC Press: Liège, Belgium, 2011.

20. Erpicum, S.; Laugier, F.; Pfister, M.; Pirotton, M.; Cicero, G.-M.; Schleiss, A.J. *Labyrinth and Piano Key Weirs II—PKW 2013*; CRC Press: Paris, France, 2013.

21. Erpicum, S.; Laugier, F.; Ho Ta Khanh, M.; Pfister, M. *Labyrinth and Piano Key Weirs III—PKW 2017*; CRC press: Qui Nhơn, Vietnam, 2017.

22. Lempérière, F. New Labyrinth Weirs Triple the Spillways Discharge–Data for an Easy Design of PK Weir. 2013. Available online: http://www.hydrocoop.org/new-labyrinth-weirs-triple-the-spillways-discharge/ (accessed on 31 July 2021).

23. Laugier, F.; Pralong, J.; Blancher, B. Influence of structural thickness of sidewalls on PKW spillway discharge capacity. In *Labyrinth and Piano Key Weirs—PKW 2011*; CRC press: Liège, Belgium, 2011; pp. 159–165.

24. Leite Ribeiro, M.; Pfister, M.; Schleiss, A.J.; Boillat, J.-L. Hydraulic design of A-type piano key weirs. *J. Hydraul. Res.* **2012**, *50*, 400–408. [CrossRef]

25. Kabiri-Samani, A.; Javaheri, A. Discharge coefficients for free and submerged flow over Piano Key weirs. *J. Hydraul. Res.* **2012**, *50*, 114–120. [CrossRef]

26. Cicero, G.; Delisle, J. Effects of the crest shape on the discharge efficiency of a type A piano key weir. In *Labyrinth and Piano Key Weirs II—PKW 2013*; CRC Press: Paris, France, 2013; pp. 41–48.

27. Machiels, O.; Pirotton, M.; Pierre, A.; Dewals, B.; Erpicum, S. Experimental parametric study and design of Piano Key Weirs. *J. Hydraul. Res.* **2014**, *52*, 326–335. [CrossRef]

28. Safarzadeh, A.; Noroozi, B. 3D hydrodynamics of trapezoidal piano key spillways. *Int. J. Civ. Eng.* **2017**, *15*, 89–101. [CrossRef]

29. Mehboudi, A.; Attari, J.; Hosseini, S. Experimental study of discharge coefficient for trapezoidal piano key weirs. *Flow Meas. Instrum.* **2016**, *50*, 65–72. [CrossRef]

30. Cicero, G.; Delisle, J.; Lefebvre, V.; Vermeulen, J. Experimental and numerical study of the hydraulic performance of a trapezoidal Piano Key weir. In *Labyrinth and Piano Key Weirs II—PKW 2013*; CRC Press: Paris, France, 2013; pp. 265–272.

31. Machiels, O.; Erpicum, S.; Dewals, B.J.; Archambeau, P.; Pirotton, M. Experimental observation of flow characteristics over a Piano Key Weir. *J. Hydraul. Res.* **2011**, *49*, 359–366. [CrossRef]

32. Li, S.; Li, G.; Jiang, D. Physical and Numerical Modeling of the Hydraulic Characteristics of Type-A Piano Key Weirs. *J. Hydraul. Eng.* **2020**, *146*, 06020004. [CrossRef]

33. Denys, F.; Basson, G.; Strasheim, J. Fluid structure interaction of piano key weirs. In *Labyrinth and Piano Key Weirs III—PKW 2017*; CRC Press: Qui Nhơn, Vietnam, 2017; pp. 119–126.

34. Denys, F.J.M. Investigation into Flow-Induced Vibrations of Piano Key Weirs. Ph.D. Thesis, Stellenbosch University, Stellenbosch, South Africa, 2019.

35. Lefebvre, V.; Vermeulen, J.; Blancher, B. Influence of geometrical parameters on PK-Weirs discharge with 3D numerical analysis. In *Labyrinth and Piano Key Weirs II–PKW 2013*; CRC press: Paris, France, 2013; pp. 49–56.

36. Li, S.; Li, G.; Jiang, D.; Ning, J. Influence of auxiliary geometric parameters on discharge capacity of piano key weirs. *Flow Meas. Instrum.* **2020**, *72*, 101719. [CrossRef]

37. Denys, F.J.; Basson, G.R. Unsteady Hydrodynamic Behavior at Piano Key Weirs. *J. Hydraul. Eng.* **2020**, *146*, 04020028. [CrossRef]

38. Kumar, B.; Kadia, S.; Ahmad, Z. Sediment Movement over Type A Piano Key Weirs. *J. Irrig. Drain. Eng.* **2021**, *147*, 04021018. [CrossRef]

39. Pralong, J.; Montarros, F.; Blancher, B.; Laugier, F. A sensitivity analysis of Piano Key Weirs geometrical parameters based on 3D numerical modeling. In *Labyrinth and Piano Key Weirs—PKW 2011*; CRC Press: Liège, Belgium, 2011; pp. 133–139.

40. Machiels, O. Experimental Study of the Hydraulic Behavior of Piano Key Weirs. Ph.D. Thesis, University of Liège, Belgium, 2012.

41. Crookston, B.; Tullis, B. Labyrinth weirs: Nappe interference and local submergence. *J. Irrig. Drain. Eng.* **2012**, *138*, 757–765. [CrossRef]

42. Crookston, B.; Tullis, B. Hydraulic design and analysis of labyrinth weirs. II: Nappe aeration, instability, and vibration. *J. Irrig. Drain. Eng.* **2013**, *139*, 371–377. [CrossRef]

43. Bilhan, O.; Emiroglu, M.E.; Miller, C.J.; Ulas, M. The evaluation of the effect of nappe breakers on the discharge capacity of trapezoidal labyrinth weirs by ELM and SVR approaches. *Flow Meas. Instrum.* **2018**, *64*, 71–82. [CrossRef]

44. Mehboudi, A.; Attari, J.; Hosseini, S.A. Flow regimes over trapezoidal Piano Key Weirs. In *Labyrinth and Piano Key Weirs III—PKW 2017*; CRC Press: Qui Nhơn, Vietnam, 2017; pp. 65–73.

45. Vermeulen, J.; Lassus, C.; Pinchard, T. Design of a piano key weir aeration network. In *Labyrinth and Piano Key Weirs III—PKW 2017*; CRC press: Qui Nhơn, Vietnam, 2017; pp. 127–133.
46. Lombaard, J. Evaluation of the Influence of Aeration on the Discharge Capacity and Flow Induced Vibrations of Piano Key Weir Spillways. Master's Thesis, Stellenbosch University, Stellenbosch, South Africa, 2020.
47. Ettema, R. *Hydraulic Modeling: Concepts and Practice*; ASCE: Reston, VA, USA, 2013.
48. Haghnazar, H.; Saneie, M. Impacts of pit distance and location on river sand mining management. *Modeling Earth Syst. Environ.* **2019**, *5*, 1463–1472. [CrossRef]
49. Sangsefidi, Y.; Torabi, M.; Tavakol-Davani, H. Discussion on "Laboratory investigation of the discharge coefficient of flow in arced labyrinth weirs with triangular plans" by Monjezi et al. (2018). *Flow Meas. Instrum.* **2020**, *72*, 101709. [CrossRef]
50. Pfister, M.; Battisacco, E.; De Cesare, G.; Schleiss, A.J. Scale effects related to the rating curve of cylindrically crested Piano Key weirs. In *Labyrinth and Piano Key Weirs II—PKW 2013*; CRC press: Paris, France, 2013; pp. 73–82.
51. Erpicum, S.; Tullis, B.P.; Lodomez, M.; Archambeau, P.; Dewals, B.J.; Pirotton, M. Scale effects in physical piano key weirs models. *J. Hydraul. Res.* **2016**, *54*, 692–698. [CrossRef]
52. Haghnazar, H.; Hashemzadeh Ansar, B.; Amini, R.; Saneie, M. Experimental study on appropriate location of river material mining pits regarding extraction and utilization. *J Min. Environ.* **2019**, *10*, 163–175.
53. Falvey, H.T. *Hydraulic Design of Labyrinth Weirs*; ASCE: Reston, VA, USA, 2002.
54. Debo, T.; Reese, A. Stormwater management programs. In *Municipal Stormwater Management*; CRC Press: Boca Raton, FL, USA, 2003.
55. Wahl, T.L. Analyzing ADV data using WinADV. In Proceedings of the Joint Conference on Water Resource Engineering and Water Resources Planning and Management 2000, Minneapolis, MN, USA, 30 July–2 August 2000; pp. 1–10.
56. Leite Ribeiro, M.; Pfister, M.; Schleiss, A.J. Overview of Piano Key weir prototypes and scientific model investigations. In *Labyrinth and Piano Key Weirs II—PKW 2013*; CRC press: Paris, France, 2013; pp. 273–281.
57. Erpicum, S.; Archambeau, P.; Dewals, B.; Pirotton, M. Hydraulics of piano key weirs: A review. In *Labyrinth and Piano Key Weirs III—PKW 2017*; CRC Press: Qui Nhơn, Vietnam, 2017; pp. 27–36.